

# Study of dependence of kinetic freezeout temperature on production cross-section of the particles in various centrality intervals in Au-Au and Pb-Pb collisions at high energies

M. Waqas<sup>1,\*</sup>, G. X. Peng<sup>1,2 †</sup>

<sup>1</sup> School of Nuclear Science and Technology, University of Chinese Academy of Sciences, Beijing 100049, China,

<sup>2</sup> Theoretical Physics Center for Science Facilities, Institute of High Energy Physics, Beijing 100049, China

**Abstract:** Transverse momentum spectra of  $\pi^+$ ,  $p$ ,  $\Lambda$ ,  $\Xi$  or  $\Xi^+$ ,  $\Omega$  or  $\bar{\Omega}^+$  and deuteron ( $d$ ) in different centrality intervals in nucleus-nucleus collision at center of mass energy are analyzed by the blast wave model with Boltzmann Gibbs statistics. We extracted Kinetic freeze out temperature, transverse flow velocity and kinetic freezeout volume from the transverse momentum spectra of the particles. It is observed that the non-strange and strange (multi-strange) particles freezeout separately due to different reaction cross-sections. While the freezeout volume and transverse flow velocity are mass dependent. They decrease with the rest mass of the particles. The present work reveals the scenario of double kinetic freezeout in nucleus-nucleus collisions. Furthermore, the kinetic freezeout temperature and freezeout volume are larger in central collisions than the peripheral collisions. However the transverse flow velocity remains almost unchanged from central to peripheral collisions.

**Keywords:** non-strange, strange, multi-strange, kinetic freeze-out temperature, transverse flow velocity, freeze-out volume, cross-section, centrality bins, transverse momentum spectra.

**PACS:** 12.40.Ee, 13.85.Hd, 25.75.Ag, 25.75.Dw, 24.10.Pa

## 1 Introduction

Freezeout stages are very important because they provide essential information about the emission of the particles at those stages. Generally, there are two freeze-out stages found in literature namely chemical freezeout and kinetic freezeout stage and both of them correspond to their respective temperatures. The chemical freezeout is the intermediate stage in high energy collisions where the intra-nuclear collisions among the particles are inelastic as well as the ratio of various types of particles remain unchanged, and the temperature of the particles at this stage is chemical freezeout temperature that describes the excitation degree of the system at the chemical freezeout stage. Correspondingly, the thermal/kinetic freezeout is the last but not the least stage in high energy collisions. At this stage, the intra-nuclear collisions among the particles are elastic. The transverse momentum distributions of various kinds of particles are no longer changed at thermal freezeout stage, and the temperature at this stage is called kinetic freezeout temperature.

According to thermal and statistical model [1–4], the chemical freezeout temperature ( $T_{ch}$ ) in central nucleus-

nucleus collisions increases with increase of the collisions energy from a few GeV to above 10 GeV and then saturates in an energy range from more than a dozen of GeV. At top Relativistic Heavy Ion Collider (RHIC) and Large Hadron Collider (LHC), the maximum  $T_{ch}$  is 160 MeV, although there is a slight decrease from RHIC to LHC energy, but the situation of kinetic freezeout temperature ( $T_0$ ) is complex. At first,  $T_0$  in central collisions increases with increasing the collision energy from a few GeV to above 10 GeV, but this tendency can either be saturated, decrescent or increscent. On the other hand,  $T_{ch}$  in central nucleus-nucleus collisions is a little larger than in peripheral nucleus-nucleus collisions, however, there are three possible trends of  $T_0$  from central to peripheral collisions which are; (1)  $T_0$  increase from central to peripheral collisions, (2)  $T_0$  decrease from central to peripheral collisions, and (3)  $T_0$  remains constant from central to peripheral collisions. It is very important to search for the correct trend of  $T_0$  with energy and centrality. Furthermore, there are different kinetic freezeout scenarios found in literature which include single, double, triple and multiple kinetic freezeout scenarios [5–10]. In single kinetic freezeout scenario, one set of parameters is used for the strange,

\*Corresponding author. Email (M.Waqas): waqas\_phy313@yahoo.com; waqas\_phy313@ucas.ac.cn

†Corresponding author. Email (G. X. Peng): gxpeng@ucas.ac.cn

multi-strange and non-strange particles. In double kinetic freezeout scenario, one set of parameters is used for strange (multi-strange) and other for non-strange particles, separate sets of parameters are used for strange, multi-strange and non-strange particles in triple kinetic freezeout scenario. While in multiple kinetic freezeout scenario, separate sets of parameters are used for each particle. The trend of transverse flow velocity ( $\beta_T$ ) and freezeout volume ( $V$ ) with energy is an increasing trend in most of the literatures [6, 11-16]. Most of the literature claims the decreasing (or invariant) trend of  $\beta_T$  and  $V$  from central to peripheral collisions [10, 15, 16–18].

The transverse momentum spectra ( $p_T$ ) of the particles are very important observables due to the reason that they provide very essential information about the equilibrium dynamics and isotropy of the system in high energy collisions [9]. In present work, we will analyze the  $p_T$  spectra of  $\pi^+$ ,  $p$ ,  $\Lambda$ ,  $\Xi$  ( $\Xi^+$ ),  $\Omega$  ( $\Omega^+$ ) and deuteron ( $d$ ) in nucleus-nucleus collisions at center of mass energy.

The remainder of the paper consists of the method and formalism, and results and discussion in section 2 and 3 respectively, and the summary of our main observations and conclusions are presented in section 4.

## 2 The method and formalism

There are various models suggested for the extraction of  $T_0$ ,  $V$  and  $\beta_T$ , e.g blast wave model with Boltzmann Gibbs statistics (BGBW) [19–21], blast wave model with Tsallis statistics [TBW] [22–24], an alternative method by using Tsallis statistics [25–31] and an alternative method by using blast wave model with Boltzmann Gibbs statistics [32–37]. In this work, we choose the blast wave model with Boltzmann Gibbs statistics which is phenomenological model and is used for the spectra of hadrons based on the flow of local thermal sources with global variables of temperature, volume and transverse flow velocity.

According to reference [38–40], the  $p_T$  distribution of the BGBW can be written as

$$f(p_T) = \frac{1}{N} \frac{dN}{dp_T} = C \frac{gV}{(2\pi)^2} p_T m_T \int_0^R r dr \times I_0 \left[ \frac{p_T \sinh(\rho_1)}{T_0} \right] K_1 \left[ \frac{m_T \cosh(\rho_1)}{T_0} \right], \quad (1)$$

where  $C$  stands for the normalization constant,  $g$  represents the degeneracy factor of the particles,  $V$  is the freezeout volume,  $m_T = \sqrt{p_T^2 + m_0^2}$  is the transverse mass ( $m_0$  is the rest mass of the particle),  $r$  is the radial coordinate,  $R$  is the maximum  $r$ ,  $\rho = \tanh^{-1}[\beta(r)]$

is the boost angle,  $\beta(r) = \beta_S(r/R)^{n_0}$  is a self-similar flow profile,  $\beta_S$  is the flow velocity on the surface, as mean of  $\beta(r)$ ,  $\beta_T = (2/R^2) \int_0^R r \beta(r) dr = 2\beta_S/(n_0 + 2)$  if  $n_0=2$ ,  $\beta_T=0.5\beta_S$ , because the maximum  $\beta_S$  is 1c and the maximum value of  $\beta_T$  is 0.5, but if  $n_0=1$ , then it will result in  $\beta_T = (2/3)\beta_S$ , hence the maximum  $\beta_T$  is  $(2/3)c$ . However if one use  $n_0$  as a free parameter [41], it fluctuates largely by several times increases 1 in the number of free parameters.  $I_0$  and  $K_1$  are the Bessel modified functions of the first and second kind respectively.

Eqn. (1) is not enough for the description of the whole  $p_T$  spectra, particularly, when the maximum  $p_T$  reaches to 100 GeV/c at LHC collisions [42], where several  $p_T$  regions [43] has been observed by the model analysis. These regions include the first  $p_T$  region with  $p_T < 4.5$  GeV/c, the second and third region with 4-6 GeV/c  $< p_T < 17-20$  GeV/c and  $p_T > 17-20$  GeV/c respectively. It is expected that different  $p_T$  regions are corresponding to different interacting mechanisms, such as the effects and changes by medium, nuclear transparency and the effect of number of strings etc, which are discussed in detail in [17]. Therefore, for the complete description of the whole  $p_T$ , we can use the functions such as Tsallis Levy [44, 45], the Hagedorn function [42, 46, 47] to the spectra in high and very high  $p_T$  regions and it corresponds to an the inverse power law. In this work, we used the inverse power law to describe the  $p_T$  spectra in high  $p_T$  regions, that is

$$f_H(p_T) = \frac{1}{N} \frac{dN}{dp_T} = A p_T \left( 1 + \frac{p_T}{p_0} \right)^{-n}, \quad (2)$$

where  $N$  and  $A$  represents the number of particles and normalization constant respectively, and  $p_0$  and  $n$  are the free parameters. There are several modified versions of Hagedorn function found in literature [48–54].

Generally, the two main process responsible for the contribution of  $p_T$  spectra are soft excitation (contributes soft component in low  $p_T$  region) and hard scattering process (contributes in whole  $p_T$  region). Eqn. (1) is taken into account for the soft excitation process and eqn.(2) for the hard scattering process. Eqn. (1) and (2) can be superposed by two methods i.e; (1) super position principle, where the contribution regions of components overlap each other and (2) by Hagedorn model (usual step function), when there is no overlapping of different regions of different components. According to the first method

$$f_0(p_T) = kf_S(p_T) + (1 - k)f_H(p_T), \quad (3)$$

where  $k$  represents the contribution fraction of the first component and  $(1-k)$  represents the contribution function of the second component.

The usual step function can be used to structure the superposition of the Eqn. (1) and (2). According to Hagedorn model [42, 46, 47], the usual step function can also be used for the superposition of the two functions, as

$$f_0(p_T) = A_1\theta(p_1 - p_T)f_1(p_T) + A_2\theta(p_T - p_1)f_2(p_T), \quad (4)$$

where  $A_1$  and  $A_2$  are the fraction constants which give the two components to be equal to each other at  $p_T=p_1$ .

It should be noted that soft and hard components in Eq. (3) and (4) are treated in different ways in the whole  $p_T$  region. Eq. (3) is used for the contribution of soft component in the range 0-2~3 GeV/c or a little more. However in case of the contribution of hard component, even though the main contribution in low  $p_T$  region is soft excitation process, but it covers the whole  $p_T$  region. In Eq. (4), in the range from 0 to  $p_1$  and from  $p_1$  up to maximum are the contributions of soft and hard components respectively, and there is no mixed region for the two components. In addition, we would like to point out that in the present work we have used Eq. (1) (which is a single component BGBW) only, but Eq. (3) and (4) are stated in order to present the whole methodology and treatment (if Eq. (2) is used). If we use double component BGBW, then we can use either eqn. (3) or (4) to combine the two components. //

### 3 Results and discussion

Figure 1 demonstrates the transverse momentum ( $p_T$ ) spectra,  $[(1/2\pi p_T) d^2N/dydp_T]$  or  $[1/N_{ev}(1/2\pi p_T) d^2N/dydp_T]$  of  $\pi^+$ ,  $p$ ,  $\Lambda$ ,  $\Xi^+$ ,  $\bar{\Omega}^+$  and deuteron ( $d$ ) in various centrality classes in Au-Au collisions at 62.4 GeV. The spectra is distributed in different centrality classes, e:g for  $\pi^+$  and  $p$ , 0-5%, 5-10%, 10-20%, 20-30%, 30-40%, 40-50%, 50-60%, 60-70% and 70-80%, for  $\Lambda$ , 0-5%, 5-10%, 10-20%, 20-30%, 30-40%, 40-60% and 60-80%, for  $\Xi^+$ , 0-5%, 5-10%, 10-20%, 20-40%, 40-60% and 60-80%, for  $\bar{\Omega}^+$ , 0-20%, 20-40% and 40-60% at  $|y| < 0.1$ , and for deuteron ( $d$ ), 0-10%, 10-20%, 20-40%, 40-60% and 60-80%, at  $|y| < 0.3$ . The symbols are cited from the experimental data measured by the

STAR Collaboration at Relativistic Heavy Ion collider (RHIC) [21, 55, 56]. In the figure, the curves are our fitted results with Eq. (1). The corresponding values of free parameters ( $T_0$ ,  $V$ ,  $\beta_T$  and  $n_0$ ), normalization constant ( $N_0$ ),  $\chi^2$  and number of degree of freedom (ndof) are listed in Table 1, in which the parameter trend will be analyzed and discussed later in this section. One can see that the  $p_T$  spectra of the particles are shown to obey approximately the blast wave model with Boltzmann Gibbs statistics. Furthermore, the spectra of  $\pi^+$  in 5-10%, 10-20%, 20-30%, 30-40%, 40-50%, 50-60%, 60-70% and 70-80% centrality intervals are scaled with 1/3, 1/7, 1/18, 1/40, 1/100, 1/250, 1/700 and 1/1500 respectively, while the centrality intervals 5-10%, 10-20%, 20-30%, 30-40%, 40-50%, 50-60%, 60-70% and 70-80% of  $p$  are scaled by 1/3, 1/7, 1/26, 1/60, 1/150, 1/250, 1/400 and 1/600 respectively.

Figure 2 is similar to Fig.1, but it shows the the  $p_T$  spectra of  $\pi^+$ ,  $p$ ,  $\Lambda$ ,  $\Xi$ ,  $\Omega$  and deuteron ( $d$ ) in different centrality intervals in Pb-Pb collisions at 2.76 TeV. The spectra is distributed in different centrality intervals, e:g for  $\pi^+$ , and  $p$ ; 0-5%, 5-10%, 10-20%, 20-30%, 30-40%, 40-50%, 50-60%, 60-70% 70-80% and 80-90% at  $|y| < 0.5$ , for  $\Lambda$ ,  $\Xi$ , and  $\Omega$ ; 0-10%, 10-20%, 20-40%, 40-60%, and 60-80%, for  $\Omega$ ; 0-10%, 10-20%, 20-40%, 40-60% and 60-80% at  $y = 0$ , and for deuteron ( $d$ ); 0-10%, 10-20%, 20-40%, 40-60% and 60-80%, at  $|y| < 0.5$ . The spectra of  $\pi^+$  and  $p$  in 5-10%, 10-20%, 20-30%, 30-40%, 40-50%, 50-60%, 60-70% and 70-80% centrality intervals are scaled with 1/2, 1/4, 1/6, 1/8, 1/10, 1/10, 1/10, 1/10 and 1/10 respectively. The symbols are cited from the experimental data measured by the ALICE Collaboration at Large Hadron Collider (LHC) [57-59]. In the figure, the curves are our fitted results with Eq. (1). The corresponding values of free parameters ( $T_0$ ,  $V$ ,  $\beta_T$  and  $n_0$ ), normalization constant ( $N_0$ ),  $\chi^2$  and number of degree of freedom (ndof) are listed in Table 1, in which the parameter trend will be analyzed and discussed below. One can see that the  $p_T$  spectra of the particles are shown to obey approximately the blast wave model with Boltzmann Gibbs statistics. We comment here by the way that we have used the method of least square to obtain the parameters in present work, and the fits (especially the ALICE data) to BGBW model are not good for quite abundant hadron species, such as  $\pi^+$  and protons due to the generation of non-inclusion resonance in low  $p_T$  region. In addition, we would also like to point out that the values of  $\chi^2$  varies especially in some cases in central collisions increases due to poor fitting.

Figure 3 analyze the dependence of kinetic freeze-

out temperature ( $T_0$ ) on centrality class ( $C\%$ ) and mass of the particles. Panel (a) and (b) show the result for Au-Au and Pb-Pb collisions respectively. The colored symbols represent different species of particles and the particles from left to right shows the result of  $T_0$  from central to peripheral collisions. One can see that the kinetic freezeout temperature of the emission source decreases with the decrease of centrality from central to peripheral collisions. The central collision corresponds to very violent collision due to large number of participant nucleons that makes the degree of excitation of system high and results in high temperature, but as the centrality decreases, the collision become less and less violent due to small number of particles involved in the interaction, which results in decreasing the degree of excitation of they system and correspondingly the temperature decreases. This result is consistent with [5, 6, 18, 27, 28, 29, 60], but inconsistent with [61–65]. In addition, the dependence of  $T_0$  on  $m_0$  is not clear. The pion and proton have almost same values for  $T_0$ , and similarly the strange (multi-strange) particles have almost same values for  $T_0$ . Deuteron has the largest mass and it freezeout at the same time with pion and proton. The reason maybe the production cross-section of the interacting particle. According to kinematics, the reactions with lower cross-section is supposed to be switched-off at higher temperatures/densities or earlier in time than the reactions with higher cross-sections.  $\pi^+$ ,  $p$  and  $d$  are non-strange particles, so they have the same  $T_0$ , while  $\Lambda$ ,  $\Xi(\bar{\Xi}^+)$  and  $\Omega(\bar{\Omega}^+)$  are strange flavored particles, so they have the same  $T_0$ . The non-strange particles have larger production cross-section than the strange or multi-strange particles, therefore the non-strange particles freezeout later than the strange (multi-strange) particles. This result is consistent with one of our recent work [10], however ref.[10] observed separate decoupling of strange and multi-strange also. It is noteworthy that the observed  $T_0$  at RHIC is lower than that of LHC. In addition, we would also like to point out that several previous literature studied the blast wave fit with different methods and got different results from our recent work. In the present work, the least square method is used, and we observed the double kinetic freezeout scenario, while the previous literature observed single or multiple kinetic freezeout scenario.

Figure 4 is similar to Fig. 3, but shows the dependence of transverse flow velocity ( $\beta_T$ ) on centrality class and mass of the particles. One can see that  $\beta_T$  depends on the rest mass of the particles. Greater the mass of the particle is, the smaller the transverse flow velocity. In

fact some hydrodynamic simulations observed the same velocity for all the particles flow, but they have different explanations. Besides, different model give different results. The selection of  $\beta_T$  is more technical and complex, even in some cases it depends on the range of  $p_T$ , such that the selection of ranges are different for different models. Furthermore, there is no centrality dependence of  $\beta_T$  observed in present work, as  $\beta_T$  is almost the same in the central and peripheral collisions. The reason behind this is that the collective behavior at the stage of kinetic freezeout does not change from central to peripheral collisions. However  $\beta_T$  is larger at LHC than that of RHIC.

Figure 5 is similar to Fig. 3 and 4, but shows the dependence of  $V$  on centrality class and mass of the particles. One can see that  $V$  decrease continuously from central to peripheral collisions because the central collisions correspond to large number of binary collisions due to the re-scattering of partons and hence the system with more participants reaches quickly to equilibrium state. While the number of participants decrease with the decrease of event centrality and the system goes to equilibrium state in a steady manner from central to peripheral collisions. Additionally,  $V$  depends on the mass of the particles. Greater the mass of the particle is, lower the  $V$ .  $V$  at LHC is larger than that at RHIC.

It should be noted that the situation of  $T_0$  and/or  $\beta_T$  are very complex on the basis of their dependence on centrality. The observed results can be changed by changing the model, or the same model but different method, or by changing the limits and conditions of the model, such that by changing the parameters, we can get different results. For example, if for central collisions, one use a smaller  $T_0$  and a larger  $\beta_T$ , a decreasing trend for  $T_0$  from peripheral to central collisions can be obtained. At the same time, a negative correlation between  $T_0$  and  $\beta_T$  will also be obtained. Similarly if one use a larger  $T_0$  and a smaller  $\beta_T$ , an increasing trend for  $T_0$  from peripheral to central collisions can be obtained. At the same time, a positive correlation between  $T_0$  and  $\beta_T$  will also be obtained.

## 4 Conclusions

The main observations and conclusions are summarized here.

a) The transverse momentum spectra of different particle species are analyzed by the blast wave model with Boltzmann Gibbs statistics and the bulk properties

Table 1. Values of free parameters  $T_0$  and  $\beta_T$ ,  $V$  and  $q$ , normalization constant ( $N_0$ ),  $\chi^2$ , and degree of freedom (dof) corresponding to the curves in Figs. 1–2.

Collisions	Centrality	Particle	$T_0$ (GeV)	$\beta_T$ (c)	$V$ ( $fm^3$ )	$N_0$	$n_0$	$\chi^2/\text{dof}$
Fig. 1 Au-Au 62.4 GeV	0 – 5%	$\pi^+$	$0.111 \pm 0.005$	$0.520 \pm 0.008$	$5000 \pm 193$	$0.25 \pm 0.06$	0.8	3/5
	5 – 10%	–	$0.107 \pm 0.004$	$0.518 \pm 0.008$	$4800 \pm 170$	$0.24 \pm 0.004$	1.3	7/5
	10 – 20%	–	$0.103 \pm 0.005$	$0.520 \pm 0.009$	$4615 \pm 165$	$0.185 \pm 0.004$	2.6	2/5
	20 – 30%	–	$0.098 \pm 0.006$	$0.515 \pm 0.011$	$4430 \pm 161$	$0.136 \pm 0.0005$	1.3	2/5
	30 – 40%	–	$0.095 \pm 0.004$	$0.517 \pm 0.009$	$4250 \pm 160$	$0.0975 \pm 0.004$	1.2	2/5
	40 – 50%	–	$0.090 \pm 0.006$	$0.512 \pm 0.010$	$4000 \pm 150$	$0.067 \pm 0.004$	1.8	5/5
	50 – 60%	–	$0.086 \pm 0.005$	$0.514 \pm 0.010$	$3800 \pm 150$	$0.049 \pm 0.005$	2	7/5
	60 – 70%	–	$0.081 \pm 0.005$	$0.513 \pm 0.011$	$3610 \pm 170$	$0.029 \pm 0.004$	2	1/5
Fig. 1 Au-Au 62.4 GeV	70 – 80%	–	$0.080 \pm 0.004$	$0.510 \pm 0.007$	$3400 \pm 176$	$0.015 \pm 0.005$	2	4/5
	0 – 5%	$p$	$0.113 \pm 0.006$	$0.490 \pm 0.010$	$4700 \pm 170$	$0.0165 \pm 0.003$	1.2	33/9
	5 – 10%	–	$0.109 \pm 0.005$	$0.500 \pm 0.011$	$4530 \pm 160$	$0.0094 \pm 0.0005$	1	20/9
	10 – 20%	–	$0.105 \pm 0.004$	$0.500 \pm 0.009$	$4400 \pm 155$	$0.0113 \pm 0.004$	1.2	5/9
	20 – 30%	–	$0.100 \pm 0.005$	$0.490 \pm 0.010$	$4225 \pm 140$	$0.008 \pm 0.0005$	1.3	3/9
	30 – 40%	–	$0.097 \pm 0.005$	$0.488 \pm 0.011$	$4160 \pm 150$	$0.0055 \pm 0.0004$	1.5	7/9
	40 – 50%	–	$0.093 \pm 0.005$	$0.489 \pm 0.009$	$3900 \pm 150$	$0.0035 \pm 0.0004$	0.8	3/9
	50 – 60%	–	$0.088 \pm 0.004$	$0.487 \pm 0.011$	$3700 \pm 158$	$0.0022 \pm 0.0003$	0.6	4/9
Fig. 1 Au-Au 62.4 GeV	60 – 70%	–	$0.083 \pm 0.006$	$0.480 \pm 0.012$	$3530 \pm 160$	$0.00175 \pm 0.0004$	0.3	4/9
	70 – 80%	–	$0.081 \pm 0.005$	$0.481 \pm 0.009$	$3310 \pm 130$	$0.00055 \pm 0.00005$	0.4	14/9
	0 – 5%	$\Lambda$	$0.137 \pm 0.006$	$0.470 \pm 0.009$	$4300 \pm 152$	$0.023 \pm 0.004$	0.7	1/7
	5 – 10%	–	$0.133 \pm 0.005$	$0.468 \pm 0.010$	$4120 \pm 160$	$0.002 \pm 0.0004$	0.7	1/7
	10 – 20%	–	$0.130 \pm 0.006$	$0.470 \pm 0.011$	$4000 \pm 187$	$0.00017 \pm 0.00004$	0.7	1/7
	20 – 30%	–	$0.126 \pm 0.004$	$0.465 \pm 0.010$	$3830 \pm 164$	$1 \times 10^{-5} \pm 4 \times 10^{-6}$	0.8	1/7
	30 – 40%	–	$0.123 \pm 0.004$	$0.467 \pm 0.012$	$3650 \pm 160$	$9 \times 10^{-7} \pm 5 \times 10^{-8}$	0.8	1/7
	40 – 60%	–	$0.120 \pm 0.005$	$0.460 \pm 0.011$	$3400 \pm 156$	$4 \times 10^{-8} \pm 3 \times 10^{-9}$	0.8	5/7
Fig. 1 Au-Au 62.4 GeV	60 – 80%	–	$0.117 \pm 0.005$	$0.460 \pm 0.012$	$3200 \pm 140$	$1 \times 10^{-9} \pm 5 \times 10^{-10}$	0.9	5/7
	0 – 5%	$\Xi^+$	$0.138 \pm 0.004$	$0.455 \pm 0.011$	$4150 \pm 150$	$0.0008 \pm 0.00004$	0.7	0.4/5
	5 – 10%	–	$0.134 \pm 0.005$	$0.450 \pm 0.011$	$4000 \pm 140$	$6.5 \times 10^{-5} \pm 6 \times 10^{-6}$	1	3/6
	10 – 20%	–	$0.131 \pm 0.006$	$0.452 \pm 0.012$	$3800 \pm 157$	$5.2 \times 10^{-6} \pm 4 \times 10^{-7}$	0.8	2/6
	20 – 40%	–	$0.127 \pm 0.004$	$0.450 \pm 0.010$	$3600 \pm 148$	$4.5 \times 10^{-7} \pm 6 \times 10^{-8}$	0.7	3/6
	40 – 60%	–	$0.124 \pm 0.005$	$0.453 \pm 0.010$	$3400 \pm 150$	$8.8 \times 10^{-9} \pm 5 \times 10^{-10}$	0.7	1/6
	60 – 80%	–	$0.120 \pm 0.005$	$0.450 \pm 0.009$	$3200 \pm 146$	$3.4 \times 10^{-10} \pm 5 \times 10^{-11}$	0.4	3/4
	Fig. 1 Au-Au 62.4 GeV	0 – 20%	$\Omega^+$	$0.138 \pm 0.004$	$0.440 \pm 0.008$	$4000 \pm 155$	$5.2 \times 10^{-5} \pm 5 \times 10^{-6}$	0.6
20 – 40%		–	$0.134 \pm 0.006$	$0.435 \pm 0.011$	$3800 \pm 146$	$2 \times 10^{-7} \pm 6 \times 10^{-8}$	1	1/0
40 – 60%		–	$0.127 \pm 0.005$	$0.436 \pm 0.012$	$3600 \pm 160$	$3.2 \times 10^{-9} \pm 7 \times 10^{-10}$	0.7	2/-1
0 – 10%		$d$	$0.114 \pm 0.005$	$0.400 \pm 0.011$	$3400 \pm 140$	$0.00085 \pm 0.00005$	1.6	3/7
10 – 20%		–	$0.109 \pm 0.006$	$0.395 \pm 0.010$	$3200 \pm 150$	$0.00034 \pm 0.00004$	1.6	2/7
20 – 40%		–	$0.104 \pm 0.005$	$0.396 \pm 0.011$	$3000 \pm 145$	$0.0001 \pm 0.00004$	1.5	1/7
40 – 60%		–	$0.097 \pm 0.005$	$0.393 \pm 0.012$	$2800 \pm 170$	$2 \times 10^{-5} \pm 5 \times 10^{-6}$	1.3	1/7
60 – 80%		–	$0.090 \pm 0.004$	$0.392 \pm 0.011$	$2632 \pm 150$	$2 \times 10^{-6} \pm 4 \times 10^{-7}$	0.9	22/6
Fig. 2 Pb-Pb 2.76 TeV	0 – 5%	$\pi^+$	$0.130 \pm 0.005$	$0.584 \pm 0.012$	$7000 \pm 200$	$345 \pm 36$	0.8	89/36
	5 – 10%	–	$0.127 \pm 0.006$	$0.583 \pm 0.010$	$6816 \pm 191$	$165.55 \pm 23$	0.7	158/36
	10 – 20%	–	$0.123 \pm 0.004$	$0.580 \pm 0.011$	$6650 \pm 185$	$60.55 \pm 8$	0.8	93/36
	20 – 30%	–	$0.119 \pm 0.005$	$0.581 \pm 0.010$	$6392 \pm 180$	$18.80 \pm 3$	0.9	58/36
	30 – 40%	–	$0.115 \pm 0.005$	$0.580 \pm 0.012$	$6200 \pm 185$	$6.3 \pm 0.4$	1	54/36
	40 – 50%	–	$0.112 \pm 0.006$	$0.580 \pm 0.011$	$6000 \pm 170$	$2.2 \pm 0.3$	1	92/36
	50 – 60%	–	$0.109 \pm 0.004$	$0.581 \pm 0.011$	$5843 \pm 162$	$0.66 \pm 0.04$	1	100/36
	60 – 70%	–	$0.106 \pm 0.006$	$0.579 \pm 0.010$	$5670 \pm 170$	$0.16 \pm 0.03$	1.1	197/36
	70 – 80%	–	$0.101 \pm 0.005$	$0.578 \pm 0.011$	$5500 \pm 166$	$0.04 \pm 0.005$	1.1	151/36
	80 – 90%	–	$0.098 \pm 0.004$	$0.576 \pm 0.010$	$5300 \pm 160$	$0.008 \pm 0.0004$	1.1	221/36
	0 – 5%	$p$	$0.131 \pm 0.005$	$0.570 \pm 0.010$	$6700 \pm 180$	$8 \pm 0.7$	1	58/30
	5 – 10%	–	$0.127 \pm 0.006$	$0.570 \pm 0.010$	$6500 \pm 170$	$4.05 \pm 0.5$	0.9	125/37
	10 – 20%	–	$0.123 \pm 0.005$	$0.570 \pm 0.009$	$6320 \pm 170$	$1.35 \pm 0.3$	1.1	37/33
	20 – 30%	–	$0.120 \pm 0.006$	$0.570 \pm 0.011$	$6180 \pm 160$	$0.9 \pm 0.05$	1.1	34/31
	30 – 40%	–	$0.116 \pm 0.005$	$0.565 \pm 0.012$	$6000 \pm 180$	$0.16 \pm 0.04$	1.07	17/31
	40 – 50%	–	$0.112 \pm 0.006$	$0.567 \pm 0.009$	$5830 \pm 170$	$0.05 \pm 0.004$	1.1	108/33
50 – 60%	–	$0.108 \pm 0.005$	$0.564 \pm 0.010$	$5650 \pm 165$	$0.016 \pm 0.003$	1	62/31	
60 – 70%	–	$0.104 \pm 0.005$	$0.562 \pm 0.011$	$5480 \pm 170$	$0.0045 \pm 0.0004$	1	140/34	
70 – 80%	–	$0.101 \pm 0.005$	$0.562 \pm 0.009$	$5300 \pm 180$	$0.001 \pm 0.0003$	0.9	214/36	
80 – 90%	–	$0.097 \pm 0.004$	$0.560 \pm 0.010$	$5100 \pm 180$	$0.0002 \pm 0.00003$	0.8	207/37	
Fig. 2 Pb-Pb 2.76 TeV	0 – 10%	$\Lambda$	$0.155 \pm 0.005$	$0.500 \pm 0.011$	$6000 \pm 200$	$0.13 \pm 0.03$	0.9	28/14
	10 – 20%	–	$0.152 \pm 0.006$	$0.497 \pm 0.009$	$5800 \pm 180$	$0.1 \pm 0.03$	0.8	27/14
	20 – 40%	–	$0.147 \pm 0.004$	$0.496 \pm 0.010$	$5600 \pm 180$	$0.06 \pm 0.004$	0.8	35/14
	40 – 60%	–	$0.142 \pm 0.005$	$0.495 \pm 0.011$	$5400 \pm 185$	$0.024 \pm 0.004$	0.6	124/14
	60 – 80%	–	$0.137 \pm 0.005$	$0.494 \pm 0.010$	$5200 \pm 170$	$0.0074 \pm 0.0005$	1.1	17/14
	0 – 10%	$\Xi$	$0.156 \pm 0.006$	$0.480 \pm 0.010$	$5500 \pm 200$	$0.0180 \pm 0.004$	1	16/7
Fig. 2 Pb-Pb 2.76 TeV	10 – 20%	–	$0.152 \pm 0.005$	$0.477 \pm 0.012$	$5300 \pm 180$	$0.0140 \pm 0.003$	1	37/7
	20 – 40%	–	$0.148 \pm 0.005$	$0.474 \pm 0.010$	$5126 \pm 170$	$0.0085 \pm 0.0005$	0.9	63/7
	40 – 60%	–	$0.144 \pm 0.005$	$0.473 \pm 0.009$	$4950 \pm 160$	$0.0032 \pm 0.0005$	0.8	82/7
	60 – 80%	–	$0.140 \pm 0.006$	$0.470 \pm 0.012$	$4700 \pm 180$	$0.0008 \pm 0.00005$	0.6	107/7
	0 – 10%	$\Omega$	$0.158 \pm 0.005$	$0.460 \pm 0.010$	$5000 \pm 150$	$0.0014 \pm 0.0003$	1.1	12/2
	10 – 20%	–	$0.154 \pm 0.005$	$0.458 \pm 0.009$	$4817 \pm 160$	$9.7 \times 10^{-4} \pm 4 \times 10^{-5}$	1.2	1/2
Fig. 2 Pb-Pb 2.76 TeV	20 – 40%	–	$0.150 \pm 0.004$	$0.457 \pm 0.012$	$4600 \pm 180$	$6 \times 10^{-4} \pm 6 \times 10^{-5}$	0.9	3/2
	40 – 60%	–	$0.147 \pm 0.005$	$0.456 \pm 0.010$	$4400 \pm 120$	$2 \times 10^{-4} \pm 5 \times 10^{-5}$	0.8	6/2
	60 – 80%	–	$0.143 \pm 0.004$	$0.453 \pm 0.012$	$4200 \pm 180$	$4 \times 10^{-5} \pm 5 \times 10^{-6}$	0.7	5/1
	0 – 10%	$d$	$0.133 \pm 0.005$	$0.430 \pm 0.008$	$4500 \pm 170$	$4.6 \times 10^{-4} \pm 5 \times 10^{-5}$	1.8	6/16
Fig. 2 Pb-Pb 2.76 TeV	10 – 20%	–	$0.130 \pm 0.005$	$0.428 \pm 0.011$	$4300 \pm 160$	$1.8 \times 10^{-4} \pm 4 \times 10^{-5}$	1.8	6/16
	20 – 40%	–	$0.126 \pm 0.006$	$0.426 \pm 0.009$	$4100 \pm 153$	$6.6 \times 10^{-5} \pm 4 \times 10^{-6}$	1.7	4/16
	40 – 60%	–	$0.122 \pm 0.004$	$0.423 \pm 0.011$	$3938 \pm 160$	$1.5 \times 10^{-5} \pm 5 \times 10^{-6}$	1.2	15/10
	60 – 80%	–	$0.118 \pm 0.005$	$0.422 \pm 0.012$	$3650 \pm 150$	$2.8 \times 10^{-6} \pm 4 \times 10^{-7}$	1.3	10/10

in terms of the kinetic freezeout temperature, transverse flow velocity and freezeout volume are extracted in different centrality classes in nucleus-nucleus collisions at center of mass energy.

b) It is observed that  $T_0$  is dependent on the cross-section of the interacting particle, i.e. Larger the production cross-section of the interacting particle correspond to smaller  $T_0$ .

c) A double kinetic freezeout scenario is observed due to the separate decoupling of non-strange and strange (multi-strange) particles.

d) The transverse flow velocity ( $\beta_T$ ) and kinetic freezeout volume ( $V$ ) are observed to depend on the mass of the particles, i.e. The larger the mass of the particle, the smaller  $\beta_T$  and  $V$ .

e) Kinetic freezeout temperature ( $T_0$ ) and freezeout volume ( $V$ ) decrease from central peripheral collisions due to decrease of degree of excitation of interacting system and the decrease of the number of binary collisions due to the re-scattering of partons respectively from central to peripheral collisions. While  $\beta_T$  is observed to be independent of centrality and remains almost unchanged from central to peripheral collisions because the collective behavior does at the stage of kinetic freezeout in interacting system does not change with event centrality.

f)  $T_0$ ,  $\beta_T$  and  $V$  are observed to be larger at LHC collisions than at RHIC.

g) The obtained results can be changed by changing the model, or the same model with different method or by changing the parameters used in the model.

)

### Data availability

The data used to support the findings of this study are included within the article and are cited at relevant places within the text as references.

### Compliance with Ethical Standards

The authors declare that they are in compliance with ethical standards regarding the content of this paper.

### Acknowledgements

The authors would like to thank support from the National Natural Science Foundation of China (Grant Nos. 11875052, 11575190, and 11135011).

## References

- [1] Cleymans J, Oeschler. H, Redlich. K and Wheaton. S, "Comparison of chemical freeze-out criteria in heavy-ion collisions," *Phys. Rev. C* **2006**, 73, 034905 doi:10.1103/PhysRevC.73.034905 [arXiv:hep-ph/0511094 [hep-ph]].
- [2] Andronic. A, Braun-Munzinger. P and Stachel. J, "Hadron production in central nucleus-nucleus collisions at chemical freeze-out," *Nucl. Phys. A* **2006**, 772, 167-199 doi:10.1016/j.nuclphysa.2006.03.012 [arXiv:nucl-th/0511071 [nucl-th]].
- [3] Andronic. A, Braun-Munzinger. P and Stachel. J, "The Horn, the hadron mass spectrum and the QCD phase diagram: The Statistical model of hadron production in central nucleus-nucleus collisions," *Nucl. Phys. A* **2010**, 834, 237C-240C doi:10.1016/j.nuclphysa.2009.12.048 [arXiv:0911.4931 [nucl-th]].
- [4] Andronic. A, Braun-Munzinger. P and Stachel. J, "Thermal hadron production in relativistic nuclear collisions," *Acta Phys. Polon. B* **2009**, 40, 1005-1012 [arXiv:0901.2909 [nucl-th]].
- [5] Waqas. M, Liu. F-H, Fakhraddin. S and Rahim. M. A, "Possible scenarios for single, double, or multiple kinetic freeze-out in high energy collisions," *Indian J. Phys.* **2019**, 93, 1329-1343 doi:10.1007/s12648-019-01396-9 [arXiv:1806.04312 [nucl-th]].
- [6] Waqas. M, and Li. B. C "Kinetic freeze-out temperature and transverse flow velocity in Au-Au collisions at RHIC-BES energies," *Adv. High Energy Phys.* **2020**, 2020, 1787183. [arXiv:1909.11339 [hep-ph]].
- [7] Khuntia. A, Sharma. H, Kumar Tiwari. S, Sahoo. R and Cleymans. J, "Radial flow and differential freeze-out in proton-proton collisions at  $\sqrt{s} = 7$  TeV at the LHC," *Eur. Phys. J. A* **2019**, 55, 3 doi:10.1140/epja/i2019-12669-6 [arXiv:1808.02383 [hep-ph]].
- [8] Thakur. D, Tripathy. S, Garg. P, Sahoo. R and Cleymans. J, "Indication of Differential Kinetic Freeze-out at RHIC and LHC Energies," *Acta Phys. Polon. Supp.* **2016**, 9, 329 doi:10.5506/APhysPolBSupp.9.329 [arXiv:1603.04971 [hep-ph]].
- [9] Shao. M, Yi. L, Tang. Z, Chen. H, Li. C and Xu. Z, "Examine the species and beam-energy dependence of particle spectra using Tsallis Statistics," *J. Phys. G* **2010**, 37, 085104 doi:10.1088/0954-3899/37/8/085104 [arXiv:0912.0993 [nucl-ex]].
- [10] Waqas. M, Peng. G. X and Liu. F-H "An evidence of triple kinetic freezeout scenario observed in all centrality intervals in Cu-Cu, Au-Au and Pb-Pb collisions at high energies," doi:10.1088/1361-6471 [arXiv:2101.07971 [hep-ph]].
- [11] Abelev. B *et al.* [ALICE], "Pion, Kaon, and Proton Production in Central Pb-Pb Collisions at  $\sqrt{s_{NN}} = 2.76$  TeV," *Phys. Rev. Lett.* **2012** 109, 252301

- doi:10.1103/PhysRevLett.109.252301 [arXiv:1208.1974 [hep-ex]].
- [12] Andronic. A, “An overview of the experimental study of quark-gluon matter in high-energy nucleus-nucleus collisions,” *Int. J. Mod. Phys. A* **2014**, 29, 1430047 doi:10.1142/S0217751X14300476 [arXiv:1407.5003 [nucl-ex]].
- [13] Zhang. S, Ma. Y. G, Chen. J . H and Zhong. C, “Production of Kaon and  $\Lambda$  in Nucleus-Nucleus Collisions at Ultrarelativistic Energy from a Blast-Wave Model,” *Adv. High Energy Phys.* **2015**, 2015, 460590 doi:10.1155/2015/460590 [arXiv:1411.1500 [nucl-th]].
- [14] Zhang. S, Ma. Y. G, Chen. J . H and Zhong. C, “Beam energy dependence of Hanbury-Brown-Twiss radii from a blast-wave model,” *Adv. High Energy Phys.* **2016**, 2016, 9414239 doi:10.1155/2016/9414239 [arXiv:1602.01564 [nucl-th]].
- [15] Waqas. M, Liu. F-H, Li. L. L and Alfanda. H. M “Effective (kinetic freeze-out) temperature, transverse flow velocity and kinetic freeze-out volume in high energy collisions,” *Nucl. Sci. Tech.* **2010**, 31, 109 doi:10.1007/s41365-020-00821-7 [arXiv:2001.06796 [hep-ph]].
- [16] Waqas. M, Liu. F-H, and Wazir. Z, “Dependence of temperatures and kinetic freeze-out volume on centrality in Au-Au and Pb-Pb collisions at high energy,” *Adv. High Energy Phys.* **2020**, 2020, 8198126 doi:10.1155/2020/8198126 [arXiv:2004.03773 [hep-ph]].
- [17] Waqas. M, Liu. F-H, “Centrality dependence of kinetic freeze-out temperature and transverse flow velocity in high energy nuclear collisions,” [arXiv:1806.05863 [hep-ph]].
- [18] Wang. Q and Liu. F-H, “Initial and final state temperatures of antiproton emission sources in high energy collisions,” *Int. J. Theor. Phys.* **2019**, 58, 4119-4138 doi:10.1007/s10773-019-04278-2 [arXiv:1909.02390 [hep-ph]].
- [19] Schnedermann. E, Sollfrank. J and Heinz. U. W “Thermal phenomenology of hadrons from 200-A/GeV S+S collisions,” *Phys. Rev. C* **1993**, 48, 2462-2475 doi:10.1103/PhysRevC.48.2462 [arXiv:nucl-th/9307020 [nucl-th]].
- [20] Abelev. B. I *et al.* [STAR], “Identified particle production, azimuthal anisotropy, and interferometry measurements in Au+Au collisions at  $\sqrt{s(NN)}^{1/2} = 9.2$ - GeV,” *Phys. Rev. C* **2010**, 81, 024911 doi:10.1103/PhysRevC.81.024911 [arXiv:0909.4131 [nucl-ex]].
- [21] Abelev. B. I *et al.* [STAR], “Systematic Measurements of Identified Particle Spectra in  $pp, d^+$  Au and Au+Au Collisions from STAR,” *Phys. Rev. C* **2009**, 79, 034909 doi:10.1103/PhysRevC.79.034909 [arXiv:0808.2041 [nucl-ex]].
- [22] Tang. Z, Yi. L, Ruan. L, Shao. M, Chen. H, Li. C, Mohanty. B, Sorensen. P, Tang. A and Xu. Z, “Statistical Origin of Constituent-Quark Scaling in the QGP hadronization,” *Chin. Phys. Lett.* **2013**, 30, 031201 doi:10.1088/0256-307X/30/3/031201 [arXiv:1101.1912 [nucl-ex]].
- [23] Jiang. K, Zhu. Y, Liu. W, Chen. H, Li. C, Ruan. L, Tang. Z, and Z. Xu, “Onset of radial flow in p+p collisions,” *Phys. Rev. C* **2015**, 91, 024910 doi:10.1103/PhysRevC.91.024910 [arXiv:1312.4230 [nucl-ex]].
- [24] Tang. Z, Xu. Y, Ruan. L, van Buren. G, Wang. F and Xu. Z, “Spectra and radial flow at RHIC with Tsallis statistics in a Blast-Wave description,” *Phys. Rev. C* **2009**, 79, 051901 doi:10.1103/PhysRevC.79.051901 [arXiv:0812.1609 [nucl-ex]].
- [25] Wei. H R, Liu. F H and Lacey. R. A, “Kinetic freeze-out temperature and flow velocity extracted from transverse momentum spectra of final-state light flavor particles produced in collisions at RHIC and LHC,” *Eur. Phys. J. A* **2016**, 52, 102 doi:10.1140/epja/i2016-16102-6 [arXiv:1601.07045 [hep-ph]].
- [26] Wei. H. R, Liu. F-H and Lacey. R. A, “Disentangling random thermal motion of particles and collective expansion of source from transverse momentum spectra in high energy collisions,” *J. Phys. G* **2016**, 43, 125102 doi:10.1088/0954-3899/43/12/125102 [arXiv:1509.09083 [nucl-ex]].
- [27] Lao H L, Wei. H R, Liu F H and Lacey. R. A, “An evidence of mass-dependent differential kinetic freeze-out scenario observed in Pb-Pb collisions at 2.76 TeV,” *Eur. Phys. J. A* **2016**, 52, 203 doi:10.1140/epja/i2016-16203-2 [arXiv:1601.00045 [nucl-th]].
- [28] Lao H L, Liu F H, Li B C., Duan M. Y and Lacey R A “Examining the model dependence of the determination of kinetic freeze-out temperature and transverse flow velocity in small collision system,” *Nucl. Sci. Tech.* **2018**, 29, 164 doi:10.1007/s41365-018-0504-z [arXiv:1708.07749 [nucl-th]].
- [29] Lao H L, Liu F H, Li B C., and Duan M Y “Kinetic freeze-out temperatures in central and peripheral collisions: Which one is larger?,” *Nucl. Sci. Tech.* **2018**, 29, 82 doi:10.1007/s41365-018-0425-x [arXiv:1703.04944 [nucl-th]].
- [30] Zheng. H and Zhu. L, “Comparing the Tsallis Distribution with and without Thermodynamical Description in  $p + p$  Collisions,” *Adv. High Energy Phys.* **2016**, 2016, 9632126 doi:10.1155/2016/9632126 [arXiv:1512.03555 [nucl-th]].
- [31] Cleymans. J and Worku. D, “Relativistic Thermodynamics: Transverse Momentum Distributions in High-Energy Physics,” *Eur. Phys. J. A* **2012**, 48, 160 doi:10.1140/epja/i2012-12160-0 [arXiv:1203.4343 [hep-ph]].

- [32] Takeuchi. S, Murase. K, Hirano. T, Huovinen. P and Nara. Y, “Effects of hadronic rescattering on multistrange hadrons in high-energy nuclear collisions,” *Phys. Rev. C* **2015**, 92, 044907 doi:10.1103/PhysRevC.92.044907 [arXiv:1505.05961 [nucl-th]].
- [33] Heinz U. W, Hydrodynamics at RHIC, “how well does it work, where and how does it break down?”, *Journal of Physics G: Nuclear and Particle Physics*, **2005**, 31, S717. doi: 10.1088/0954-3899/31/6/012, [arXiv:nucl-th/0412094]
- [34] Heiselberg H. and Levy A M, “Elliptic flow and HanburyBrown CTwiss correlations in noncentral nuclear collisions”, *Physical Review C*. **1999**, 59, 2716 C2727,
- [35] Russo R, “Measurement of  $D^+$  meson production in p-Pb collisions with the ALICE detector,” [arXiv:1511.04380 [nucl-ex]].
- [36] Bíró G, Barnaföldi G. G, Biró T. S, Ürmössy K and Takács Á., “Systematic Analysis of the Non-extensive Statistical Approach in High Energy Particle Collisions - Experiment vs. Theory,” *Entropy* **2017**, 19, 88 doi:10.3390/e19030088 [arXiv:1702.02842 [hep-ph]].
- [37] Sadhu. S and Ghosh. P, “Anomalous features of particle production in high-multiplicity events of  $pp$  collisions at the LHC energies,” *Phys. Rev. D* **2019**, 99, 034020 doi:10.1103/PhysRevD.99.034020 [arXiv:1901.06787 [hep-ph]].
- [38] Chatrchyan. S *et al.* [CMS], “Study of high-pT charged particle suppression in PbPb compared to  $pp$  collisions at  $\sqrt{s_{NN}} = 2.76$  TeV,” *Eur. Phys. J. C* **2012**, 72, 1945 doi:10.1140/epjc/s10052-012-1945-x [arXiv:1202.2554 [nucl-ex]].
- [39] Tsallis. C, “Possible Generalization of Boltzmann-Gibbs Statistics,” *J. Statist. Phys.* **1988**, 52, 479-487 doi:10.1007/BF01016429
- [40] Abelev B. I, Adams J, Aggarwal M. M *et al.*, “Strange particle production in p + p collisions at 200 GeV”, *Physical Review C*. **2007**, 75, 064901
- [41] Petrovici. M, Andrei C, Berceanu I, Bercuci A, Herghelegiu A and Pop A, “Recent results and open questions on collective type phenomena from A-A to pp collisions,” *AIP Conf. Proc.* **2015**, 1645, 52-60 doi:10.1063/1.4909559. [arXiv:1411.0869 [nucl-ex]].
- [42] Hagedorn R, “Multiplicities,  $p_T$  distributions and the expected hadron quark-gluon phase transition”, *La Rivista del Nuovo Cimento* **1983**, 6, 1 C50
- [43] Suleymanov M, “The meaning behind observed  $p_T$  regions at the LHC energies,” *Int. J. Mod. Phys. E* **2018**, 27, 1850008 doi:10.1142/S0218301318500088 [arXiv:1707.03420 [nucl-ex]].
- [44] Abelev B B *et al.* [ALICE], “Production of  $\Sigma(1385)^\pm$  and  $\Xi(1530)^0$  in proton-proton collisions at  $\sqrt{s} = 7$  TeV,” *Eur. Phys. J. C* **2015**, 75, 1 doi:10.1140/epjc/s10052-014-3191-x [arXiv:1406.3206 [nucl-ex]].
- [45] Odorico R, “DOES A TRANSVERSE ENERGY TRIGGER ACTUALLY TRIGGER ON LARGE P(T) JETS?,” *Phys. Lett. B* **1982**, 118, 151-154 doi:10.1016/0370-2693(82)90620-7
- [46] Arnison G, Astbury A, Aubert B *et al.*, “Transverse momentum spectra for charged particles at the CERN proton antiproton collider”, *Physics Letters B* **1982**, 118, 167 C172
- [47] Biyajima M, Mizoguchi T and Suzuki N, “Analyses of whole transverse momentum distributions in  $p\bar{p}$  and  $pp$  collisions by using a modified version of Hagedorn’s formula,” *Int. J. Mod. Phys. A* **2017**, 32, 1750057 doi:10.1142/S0217751X17500579 [arXiv:1604.01264 [hep-ph]].
- [48] Abelev B *et al.* [ALICE], “Heavy flavour decay muon production at forward rapidity in proton-proton collisions at  $\sqrt{s} = 7$  TeV,” *Phys. Lett. B* **2012**, 708, 265-275 doi:10.1016/j.physletb.2012.01.063 [arXiv:1201.3791 [hep-ex]].
- [49] Lakomov I [ALICE], “Event activity dependence of inclusive  $J/\psi$  production in p-Pb collisions at  $\sqrt{s_{NN}} = 5.02$  TeV with ALICE at the LHC,” *Nucl. Phys. A* **2014**, 931, 1179-1183 doi:10.1016/j.nuclphysa.2014.08.062 [arXiv:1408.0702 [hep-ex]].
- [50] Abelev B *et al.* [ALICE], “Inclusive  $J/\psi$  production in  $pp$  collisions at  $\sqrt{s} = 2.76$  TeV,” *Phys. Lett. B* **2012**, 718, 295-306 [erratum: *Phys. Lett. B* **748** (2015), 472-473] doi:10.1016/j.physletb.2012.10.078 [arXiv:1203.3641 [hep-ex]].
- [51] Abelev B *et al.* [ALICE], “Light vector meson production in  $pp$  collisions at  $\sqrt{s} = 7$  TeV,” *Phys. Lett. B* **2012**, 710, 557-568 doi:10.1016/j.physletb.2012.03.038 [arXiv:1112.2222 [nucl-ex]].
- [52] Abt I *et al.* [HERA-B], “ $K^*$  and phi meson production in proton-nucleus interactions at  $s^{**}(1/2) = 41.6$ -GeV,” *Eur. Phys. J. C* **2007**, 50, 315-328 doi:10.1140/epjc/s10052-007-0237-3 [arXiv:hep-ex/0606049 [hep-ex]]
- [53] De Falco A [ALICE], “Vector meson production in pp collisions at  $\sqrt{s} = 7$  TeV, measured with the ALICE detector,” *J. Phys. G* **2011**, 38, 124083 doi:10.1088/0954-3899/38/12/124083 [arXiv:1106.4140 [nucl-ex]].
- [54] Aamodt K *et al.* [ALICE], “Transverse momentum spectra of charged particles in proton-proton collisions at  $\sqrt{s} = 900$  GeV with ALICE at the LHC,” *Phys. Lett. B* **2010**, 693, 53-68 doi:10.1016/j.physletb.2010.08.026 [arXiv:1007.0719 [hep-ex]].
- [55] Aggarwal M. M *et al.* [STAR], “Strange and Multi-strange Particle Production in Au+Au Collisions at  $\sqrt{s_{NN}} = 62.4$  GeV,” *Phys. Rev. C*

- 2011**, 83, 024901 doi:10.1103/PhysRevC.83.024901 [arXiv:1010.0142 [nucl-ex]]
- [56] Adam J *et al.* [STAR], “Beam energy dependence of (anti-)deuteron production in Au + Au collisions at the BNL Relativistic Heavy Ion Collider,” Phys. Rev. C **2019**, 99, 064905 doi:10.1103/PhysRevC.99.064905 [arXiv:1903.11778 [nucl-ex]].
- [57] Abelev B *et al.* [ALICE], “Centrality dependence of  $\pi$ , K, p production in Pb-Pb collisions at  $\sqrt{s_{NN}} = 2.76$  TeV,” Phys. Rev. C **2013**, 88, 044910 doi:10.1103/PhysRevC.88.044910 [arXiv:1303.0737 [hep-ex]].
- [58] Begun V, Florkowski W and Rybczynski M, “Transverse-momentum spectra of strange particles produced in Pb+Pb collisions at  $\sqrt{s_{NN}} = 2.76$  TeV in the chemical non-equilibrium model,” Phys. Rev. C **2014**, 90, (2014), 054912 doi:10.1103/PhysRevC.90.054912 [arXiv:1405.7252 [hep-ph]].
- [59] Adam J *et al.* [ALICE], “Production of light nuclei and anti-nuclei in pp and Pb-Pb collisions at energies available at the CERN Large Hadron Collider,” Phys. Rev. C **2016**, 93, 024917 doi:10.1103/PhysRevC.93.024917 [arXiv:1506.08951 [nucl-ex]].
- [60] Waqas M and Liu F-H, “Initial, effective, and kinetic freeze-out temperatures from transverse momentum spectra in high-energy proton(deuteron)–nucleus and nucleus–nucleus collisions,” Eur. Phys. J. Plus **2020**, 135, 147 doi:10.1140/epjp/s13360-020-00213-1 [arXiv:1911.01709 [hep-ph]].
- [61] Che G. R, Gu J. B, Zhang W. C and Zheng H, “Identified particle spectra in Pb-Pb and p-Pb collisions with a modified Tsallis blast-wave model,” [arXiv:2010.14880 [nucl-th]].
- [62] Bashir I. u and Uddin S, “Centrality Dependence of  $K^*(892)^0$  and  $\phi(1020)$  Production at LHC,” Commun. Theor. Phys. **2017**, 68, 500 doi:10.1088/0253-6102/68/4/500 [arXiv:1510.05874 [hep-ph]].
- [63] Uddin S, Bhat R. A and Bashir I. u, “Study of Centrality Dependence of Transverse Momentum Spectra of Hadrons and the Freeze-out Parameters at root(sNN) of 62.4 GeV, 130 GeV and 200 GeV,” [arXiv:1412.2663 [hep-ph]].
- [64] Waqas M and Peng G. X, “Study of proton, deuteron and triton at 54.4 GeV,” [arXiv:2103.07852 [hep-ph]].
- [65] Acharya S *et al.* [ALICE], “Production of charged pions, kaons, and (anti-)protons in Pb-Pb and inelastic  $pp$  collisions at  $\sqrt{s_{NN}} = 5.02$  TeV,” Phys. Rev. C **2020**, 101, 044907 doi:10.1103/PhysRevC.101.044907 [arXiv:1910.07678 [nucl-ex]].

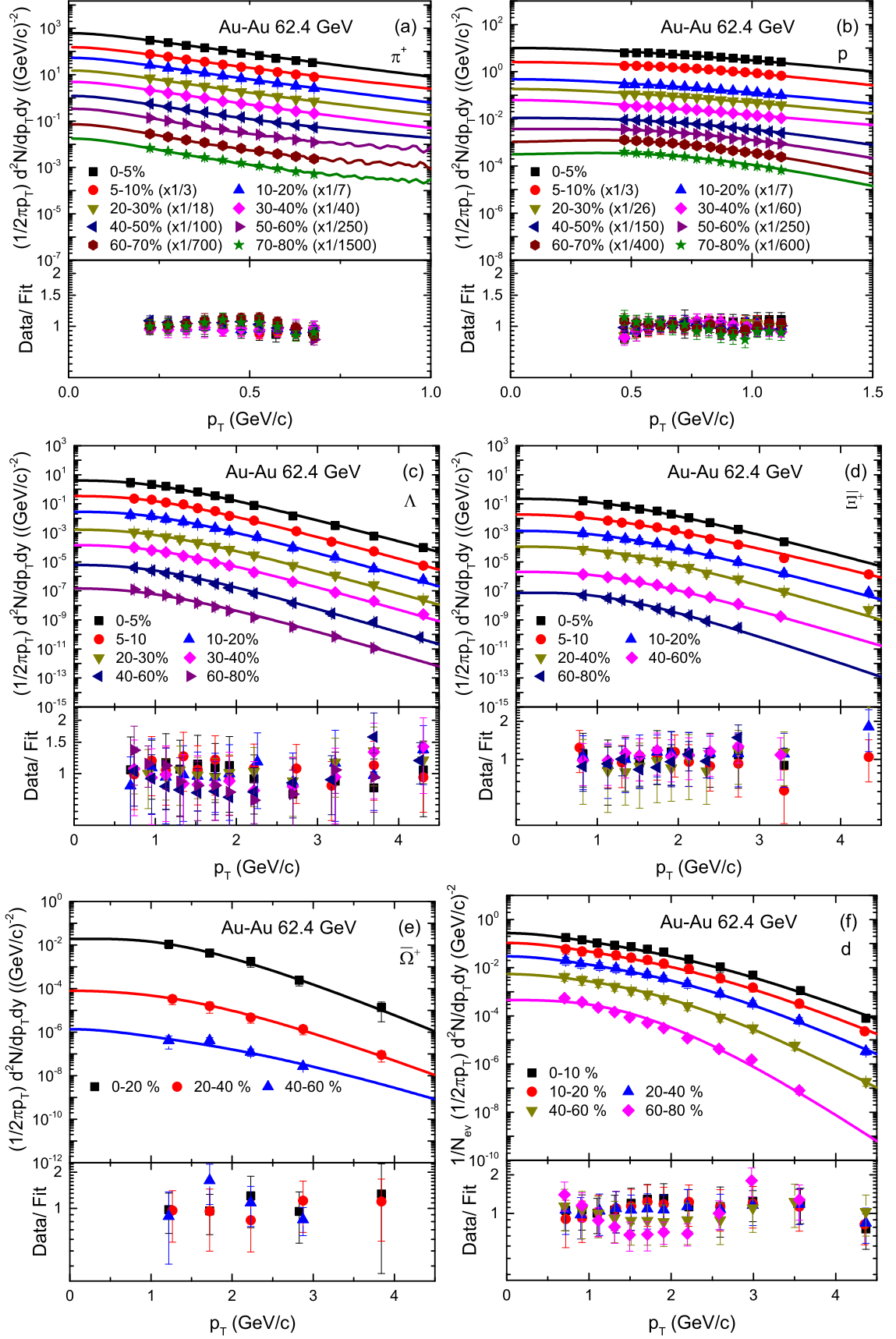


Fig. 1. Transverse momentum spectra of  $\pi^+$ ,  $p$ ,  $\Lambda$ ,  $\Xi^-$  and  $\Omega^-$  rapidity at  $|y| < 0.1$ , and deuteron ( $d$ ) at rapidity  $|y| < 0.3$ , produced in different centrality intervals in Au-Au collisions at 62.4 GeV. Different symbols represent the  $p_T$  spectra of different particles measured by the STAR collaboration [21, 55, 56] and the curves are our fitted results with BGBW model. The corresponding results of data/fit is presented in each panel.

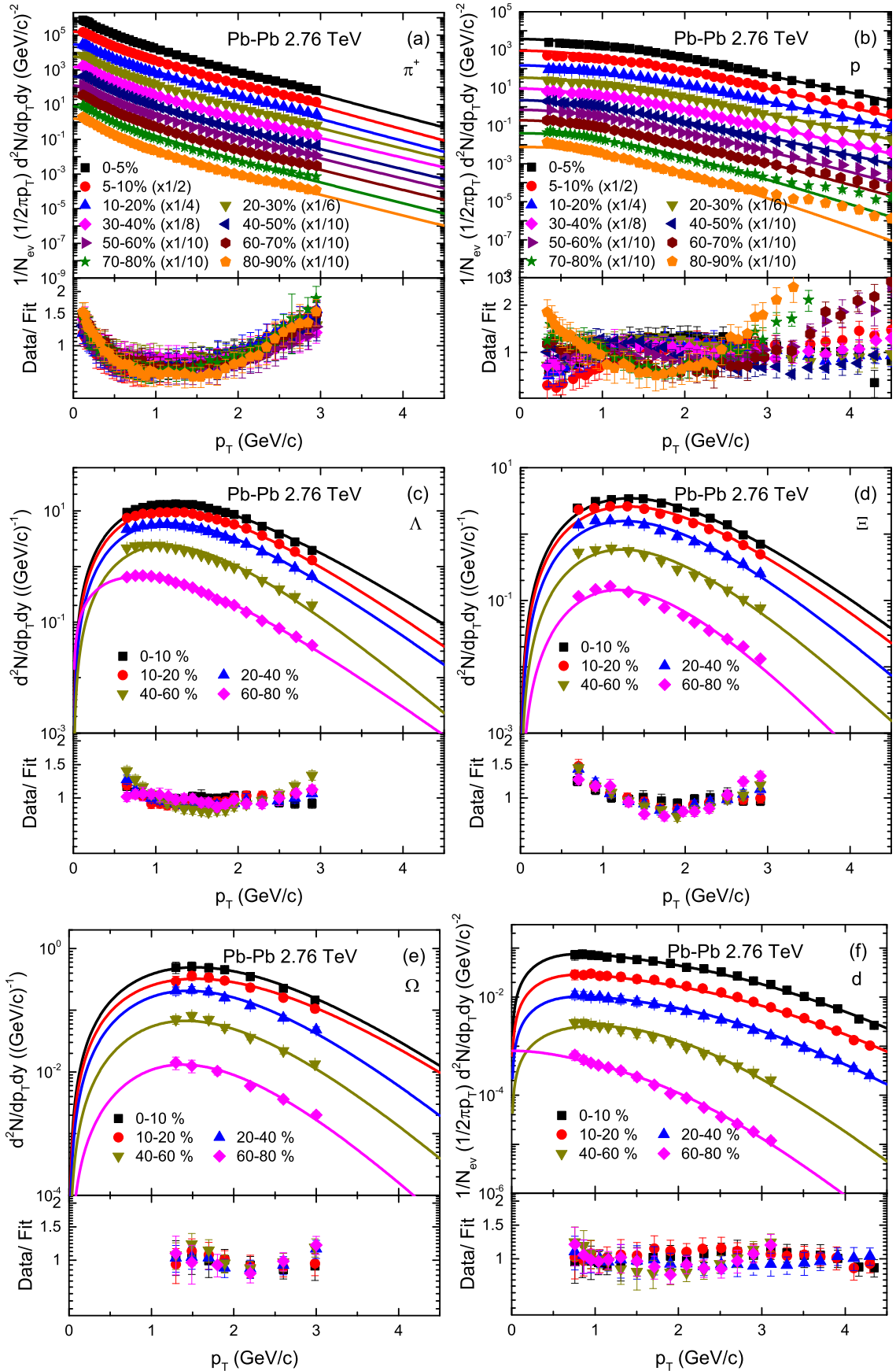


Fig. 2. Transverse momentum spectra of  $\pi^+$ ,  $p$ ,  $\Lambda$ ,  $\Xi$ ,  $\Omega$  and deuteron ( $d$ ) produced in different centrality intervals in Pb-Pb collisions at 2.76 TeV at rapidity  $|y| < 0.5$ . Different symbols represent the  $p_T$  spectra of different particles measured by the ALICE collaboration [57–59] and the curves are our fitted results with BGBW model. The corresponding results of data/fit is presented in each panel.

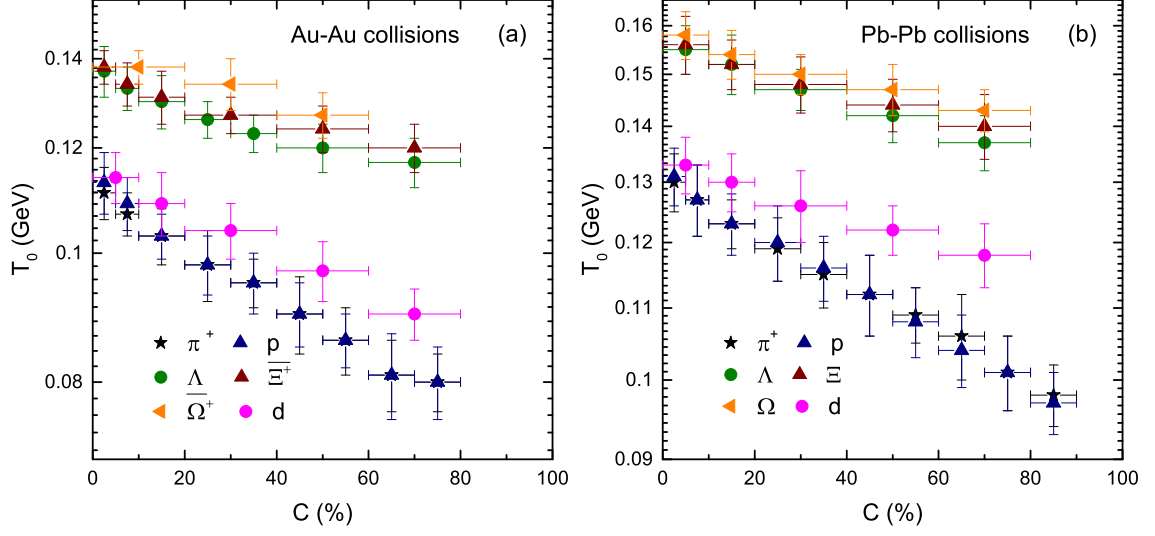


Fig. 3. Dependence of  $T_0$  on centrality class ( $C\%$ ) and rest mass ( $m_0$ ) of the particle.

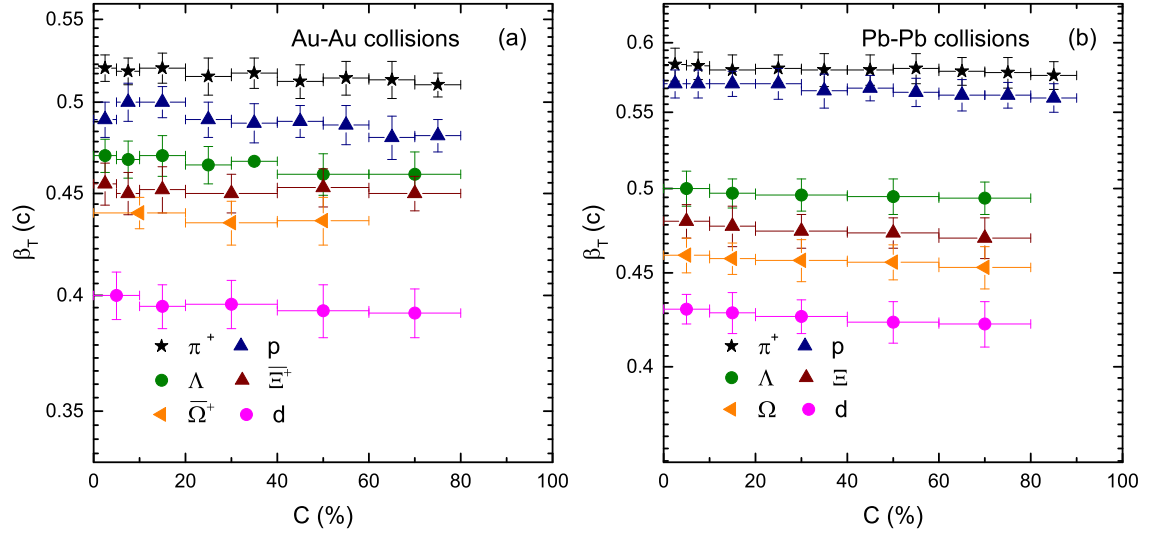


Fig. 4. Dependence of  $\beta_T$  on centrality class ( $C\%$ ) and rest mass ( $m_0$ ) of the particle.

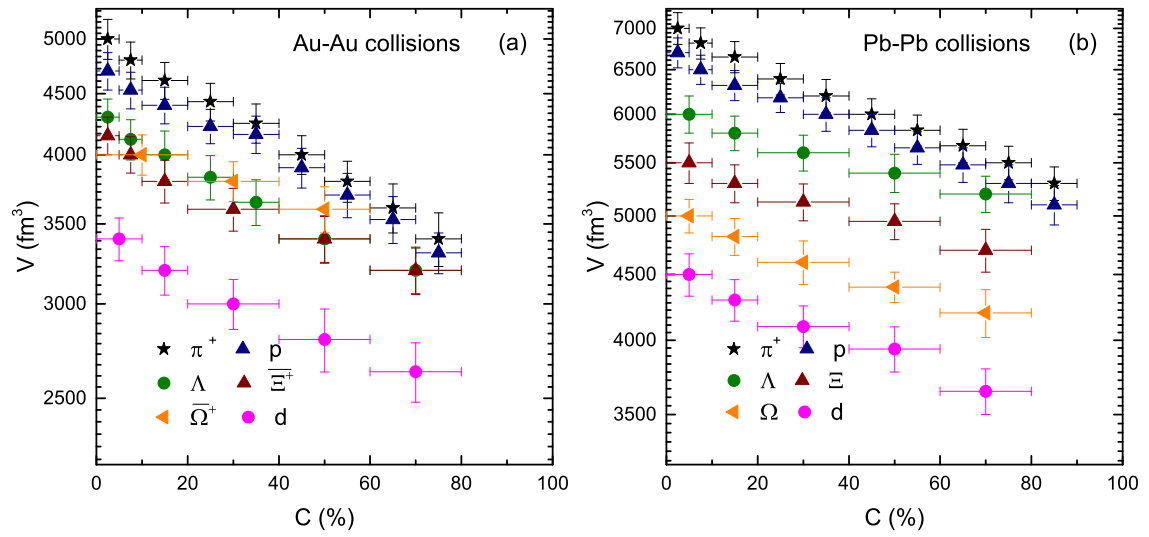


Fig. 5. Dependence of  $V$  on centrality class ( $C\%$ ) and rest mass ( $m_0$ ) of the particle.